

Integrable models of galactic discs with double nuclei

M. A. Jalali [★] & A. R. Rafiee

Institute for Advanced Studies in Basic Sciences, P.O. Box 45195-159, Gava Zang, Zanjan, IRAN

22 October 2018

ABSTRACT

We introduce a new class of 2-D mass models, whose potentials are of Stäckel form in elliptic coordinates. Our model galaxies have two separate strong cusps that form double nuclei. The potential and surface density distributions are locally axisymmetric near the nuclei and become *highly* non-axisymmetric outside the nucleus. The surface density diverges toward the cuspy nuclei with the law $\Sigma \propto r^{-2}$. Our model is sustained by four general types of regular orbits: *butterfly*, *nucleophilic banana*, *horseshoe* and *aligned loop* orbits. Horseshoes and nucleophilic bananas support the existence of cuspy regions. Butterflies and aligned loops control the non-axisymmetric shape of outer regions. Without any need for central black holes, our distributed mass models resemble the nuclei of M31 and NGC4486B. It is also shown that the self-gravity of the stellar disc can prevent the double nucleus to collapse.

Key words: stellar dynamics – galaxies: kinematics and dynamics – galaxies: nuclei – galaxies: structure.

1 INTRODUCTION

Hubble Space Telescope (HST) data revealed that M31 and NGC4486B have double nuclei (Lauer et al. 1996, hereafter L96; Tremaine 1995, hereafter T95). M31 has a bright nucleus (P1) displaced from the centre of the isophotal lines of outer regions and a fainter nucleus (P2) just at the centre. NGC4486B exhibits a similar structure with a minor difference: The centre of outer isophotes falls between P1 and P2. There are some explanations for the emergence of the double nuclei of these galaxies, among which the eccentric disc model of T95 has been more impressive. In the model of T95, a central black hole (BH) enforces stars to move on “aligned” Keplerian orbits, which may elongate in the same direction as the long-axis of the model. Stars moving on aligned Keplerian orbits linger near apoapsis and may result in P1. The mass of central “supermassive” BH should be much greater than the mass of neighboring disc. Otherwise, the asymmetric growth of P1 won’t allow the BH to remain in equilibrium.

Goodman & Binney (1984) showed that central massive objects enforce the orbital structure of stellar systems to evolve towards a steady symmetric state. This result was then confirmed by the findings of Merritt & Quinlan (1998) and Jalali (1999, hereafter J99) in their study of elliptical galaxies with massive nuclear BHs. Within the BH sphere of influence, highly non-axisymmetric structure can only exist for a narrow range of BH mass (J99). The results of J99

show that *long-axis tube* orbits of non-axisymmetric discs with central massive BHs, elongate in the both \pm directions of long-axis. Thus, the probabilities for the occurrence of two bright regions, in both sides of BH along the long-axis, are equal (these bright regions are supposed to be formed near the apogee of long-axis tubes). By this hypothesis one can interpret the double structure of NGC4486B by placing a supermassive BH between P1 and P2. However, some disadvantages arise in the case of M31. In the nucleus of M31, the formation of P1 can still be deduced from the behavior of long-axis tubes. But, there is no mathematical proof for the “coexistence” of P1 and P2 when the centre of P2 coincides with BH’s location.

In this paper we attempt to create a model based on the self-gravity of stellar discs to show that systems with double nuclei can exist even in the absence of central BHs. Especial cases of our non-scale-free planar models are eccentric discs, which display a collection of properties expected in self-consistent cuspy systems. Our models are of Stäckel form in elliptic coordinates (e.g., Binney & Tremaine 1987) for which the Hamilton-Jacobi equation separates and stellar orbits are regular.

In most galaxies, density diverges toward the centre in a power-law cusp. In the presence of a cusp, regular box orbits are destroyed and replaced by chaotic orbits (Gerhard & Binney 1985). Through a fast mixing phenomenon, stochastic orbits cause the orbital structure to become axisymmetric at least near the centre (Merritt & Valluri 1996). These results are confirmed by the findings of Zhao et al. (1999, hereafter Z99). Their study reveals that highly non-axisymmetric, scale-free mass models can not be constructed

[★] E-mail: jalali@iasbs.ac.ir

self-consistently. Near the cuspy nuclei, the potential functions of our distributed mass models are proportional to r^{-1} as $r \rightarrow 0$. So, we attain an axisymmetric structure near the nuclei which is consistent with the mentioned nature of density cusps. The slope of potential function changes sign as we depart from the centre and our model galaxies considerably become non-axisymmetric. Non-axisymmetric structure is supported by *butterfly* and *aligned loop* orbits. Close to the larger nucleus, loop orbits break down and give birth to a new family of orbits, *horseshoe* orbits, which in turn generate *nucleophilic banana* orbits. Stars moving in horseshoe and banana orbits lose their kinetic energy as they approach to the nuclei and contribute a large amount of mass to form cuspy regions.

2 THE MODEL

Let us introduce the following family of planar potentials expressed in the usual (x, y) cartesian coordinates:

$$\Phi = K \frac{(r_1 + r_2)^\gamma - \beta(r_1 - r_2)|r_1 - r_2|^{\gamma-1}}{2r_1r_2}, \quad (1)$$

$$r_1^2 = (x + a)^2 + y^2, \quad r_2^2 = (x - a)^2 + y^2, \quad (2)$$

where $a, K > 0$, $0 \leq \beta \leq 1$ and $2 < \gamma < 3$ are constant parameters. The points $(x = -a, y = 0)$ and $(x = a, y = 0)$ are the nuclei of our 2-D model. We call them P1 and P2, respectively. The distance between P1 and P2 is equal to $2a$. The surface density distribution corresponding to Φ is determined by (Binney & Tremaine 1987)

$$\Sigma(x', y') = \frac{1}{4\pi^2 G} \iint \frac{(\nabla^2 \Phi) dx dy}{\sqrt{(x' - x)^2 + (y' - y)^2}}. \quad (3)$$

It is a difficult task to evaluate (3) analytically. So, we have adopted a numerical technique to calculate this double integral. The functions Φ and Σ are cuspy at P1 and P2. To verify this, we investigate the behavior of Φ and Σ near the nuclei ($r_1 \rightarrow 0$ and $r_2 \rightarrow 0$). Sufficiently close to P1, we have $r_1 \ll r_2$ that simplifies (1) as follows

$$\Phi = \frac{Kr_2^{\gamma-1} (1 + \frac{r_1}{r_2})^\gamma + \beta(1 - \frac{r_1}{r_2})^\gamma}{2r_1}. \quad (4)$$

We expand $(1 + \frac{r_1}{r_2})^\gamma$ and $(1 - \frac{r_1}{r_2})^\gamma$ in terms of r_1/r_2 to obtain

$$\Phi = \frac{Kr_2^{\gamma-1}}{2r_1} \sum_{n=0}^{\infty} \left[\frac{(1 + (-1)^n \beta) \Gamma(\gamma + 1)}{n! \Gamma(\gamma - n + 1)} \left(\frac{r_1}{r_2}\right)^n \right], \quad (5)$$

where Γ is the well known Gamma function. As r_1 tends to zero, r_2 is approximated by $2a$ and $r_1/r_2 \rightarrow 0$. Therefore, Equation (5) reads

$$\Phi \approx \frac{Q(1 + \beta)}{r_1}, \quad Q = \frac{1}{2} K (2a)^{\gamma-1}, \quad (6)$$

from which one concludes

$$\Sigma \propto Q(1 + \beta)r_1^{-2}. \quad (7)$$

Similarly, it can readily be shown that the following approximations hold close to P2 ($r_2/r_1 \rightarrow 0$),

$$\Phi \approx \frac{Q(1 - \beta)}{r_2}, \quad (8)$$

$$\Sigma \propto Q(1 - \beta)r_2^{-2}. \quad (9)$$

In distant regions, when $r \gg a$ (with $r^2 = x^2 + y^2$), the potential function is approximated by

$$\Phi \approx 2^{\gamma-1} K r^{\gamma-2}. \quad (10)$$

Correspondingly,

$$\Sigma \propto r^{\gamma-3}. \quad (11)$$

This shows that the surface density falls off outward if $\gamma < 3$. Besides, orbits will be bounded if the potential Φ is concave in outer regions. This requirement implies $\gamma > 2$. Thus, we are restricted to $2 < \gamma < 3$. In Fig. 1, we have plotted the isocontours of Φ and Σ for $\gamma = 2.8$, $a = 0.5$ and several choices of β . The 3-D views of Φ and Σ have also been demonstrated in Fig. 2. In § 5, the potential surface of Fig. 2a will be referred as *potential hill*.

Figs. 1 and 2 assure that the potential and surface density functions are cuspy at P1 and P2. Regardless of the values of constant parameters, the potential Φ has a local minimum at $(x = 0, y = 0)$. This minimum point can easily be distinguished in Figs. 1a, 1b and 1c. As the surface density isocontours show, the cuspy zones are disjointed by two separatrices that transversally intersect each other at a saddle point located on the x -axis between P1 and P2. The x -coordinate of this point can be determined through solving

$$\frac{\partial \Sigma(x, y)}{\partial x} = 0, \quad y = 0, \quad (12)$$

for x .

The parameter β controls the sizes of cuspy zones around P1 and P2. For $\beta = 0$, the sizes of two cuspy zones are equal and the model has reflection symmetries with respect to coordinate axes. For $0 < \beta < 1$, the size of cuspy zone near P1 is larger than that of P2 and the model is only symmetric with respect to the x -axis. The cuspy region around P2 is shrunk to zero size when $\beta = 1$ and we attain an eccentric disc with a single nuclear cusp. Equations (6) through (9) show that the potential and surface density functions are approximately axisymmetric in the neighborhood of P1 and P2. As we move outward, a ‘‘highly’’ non-axisymmetric structure occurs. For the large values of r , the surface density monotonically decreases outward and our model galaxies become rounder again. Our mass models are indeed hybrid ones, which reflect the properties of density cusps and non-axisymmetric systems, simultaneously. The centre of outer surface density isocontours falls at the middle of the centerline of P1 and P2. Nevertheless, the effective cuspy zones around P1 and P2 have different sizes.

In what follows, we show that the potential Φ is of Stäckel form in elliptic coordinates. We then classify possible orbit families, all of which are non-chaotic.

3 ORBIT FAMILIES

We carry out a transformation to elliptic coordinates as follows

$$x = a \cosh u \cos v, \quad (13)$$

$$y = a \sinh u \sin v, \quad (14)$$

where $u \geq 0$ and $0 \leq v \leq 2\pi$. The curves of constant u and v are confocal ellipses and hyperbolas, respectively. P1 and

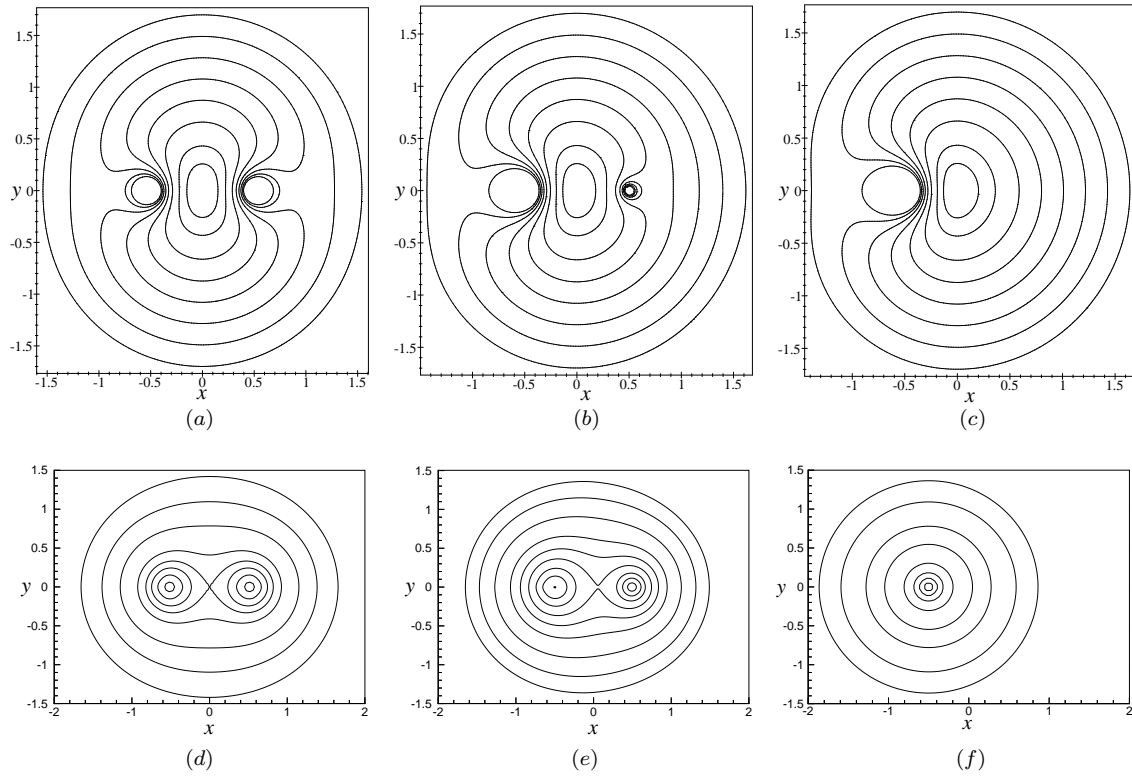


Figure 1. The potential (Φ) and surface density (Σ) isocontours for $\gamma = 2.8$, $a = 0.5$ and $K = 0.2$. Figures (a), (b) and (c) show the potential isocontours for $\beta = 0$, $\beta = 0.75$ and $\beta = 1$, respectively. The corresponding surface density isocontours are illustrated in Figures (d),(e) and (f).

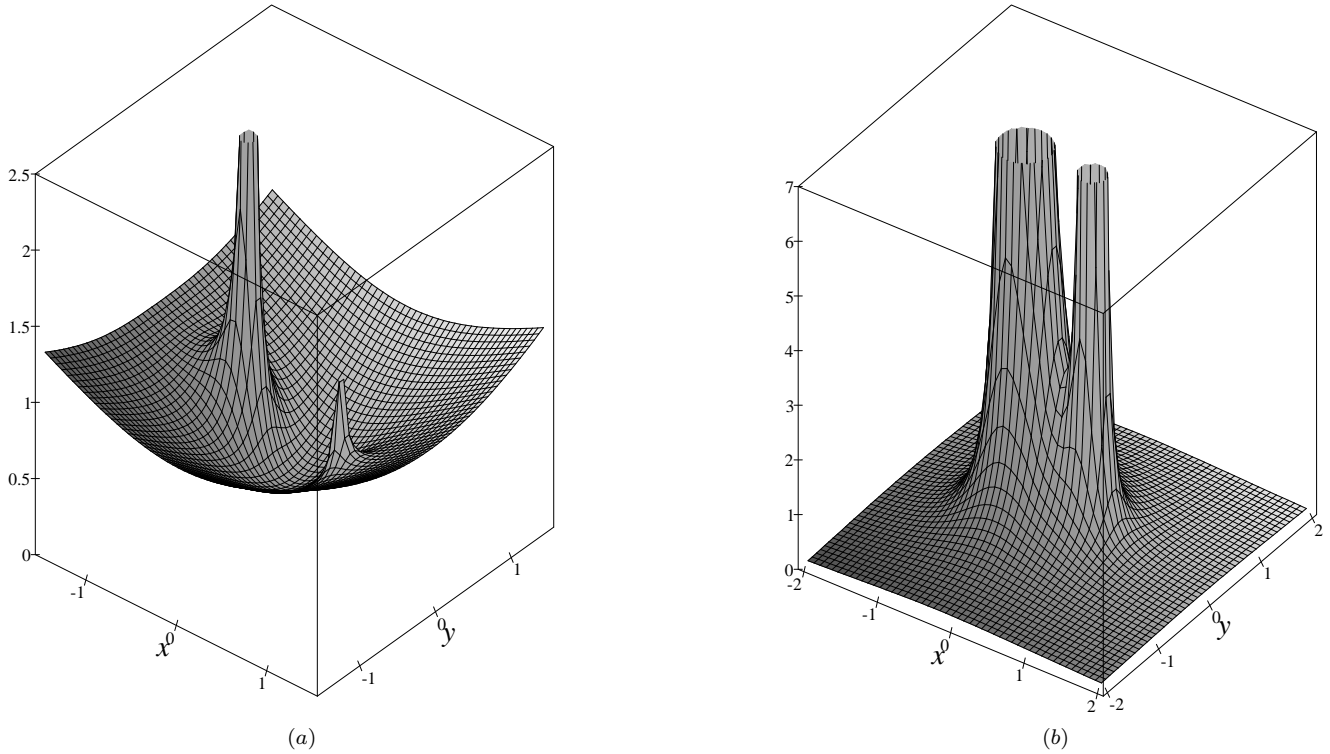


Figure 2. The 3-D views of Φ and Σ for $\gamma = 2.8$, $a = 0.5$, $K = 0.2$ and $\beta = 0.75$. (a) the potential function (b) the surface density distribution.

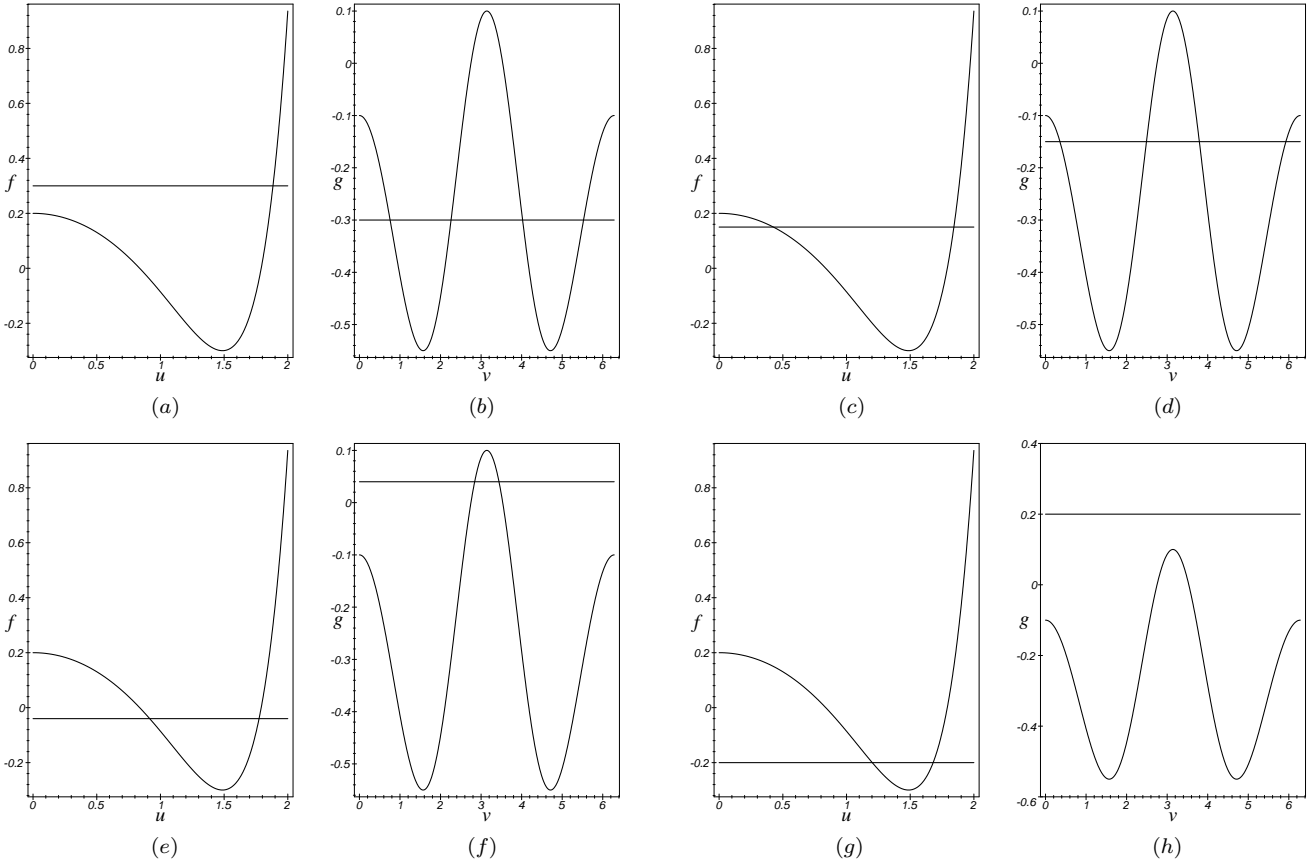


Figure 3. The graphs of $f(u)$ and $g(v)$ for $\beta = 0.5$, $\gamma = 2.8$, $C = 0.2$, $E = 1.1$ and $a = 0.5$. The horizontal lines indicate the levels of I_2 and $-I_2$ in the graphs of $f(u)$ and $g(v)$, respectively. (a) $I_2 = 0.3$ (b) $-I_2 = -0.3$ (c) $I_2 = 0.15$ (d) $-I_2 = -0.15$ (e) $I_2 = -0.04$ (f) $-I_2 = 0.04$ (g) $I_2 = -0.2$ (h) $-I_2 = 0.2$.

P2 are the foci of these curves. In the new coordinates, the motion of a test star is determined by the Hamiltonian

$$\mathcal{H} = \frac{1}{2a^2(\sinh^2 u + \sin^2 v)}(p_u^2 + p_v^2) + \Phi(u, v), \quad (15)$$

where p_u and p_v denote the canonical momenta and

$$\Phi = \frac{F(u) + G(v)}{2a^2(\sinh^2 u + \sin^2 v)}, \quad (16)$$

$$F(u) = C(\cosh u)^\gamma, \quad (17)$$

$$G(v) = -C\beta \cos v |\cos v|^{\gamma-1}, \quad (18)$$

$$C = K(2a)^\gamma.$$

The transformed potential (16) is of Stäckel form for which the Hamilton-Jacobi equation separates and yields the second integral of motion, I_2 . We obtain

$$I_2 = p_u^2 - 2a^2 E \sinh^2 u + F(u), \quad (19)$$

or equivalently

$$-I_2 = p_v^2 - 2a^2 E \sin^2 v + G(v), \quad (20)$$

where E is the total energy of the system, $E \equiv \mathcal{H}$. The potential function (Φ) is positive everywhere. Hence, we immediately conclude $E > 0$.

Having the two isolating integrals E and I_2 , one can find the possible regions of motion by employing the positiveness of p_u^2 and p_v^2 in (19) and (20). We define the following func-

tions:

$$f(u) = -2a^2 E \sinh^2 u + F(u), \quad (21)$$

$$g(v) = -2a^2 E \sin^2 v + G(v). \quad (22)$$

Since $p_u^2 \geq 0$ and $p_v^2 \geq 0$, one can write

$$I_2 - f(u) \geq 0, \quad (23)$$

$$-I_2 - g(v) \geq 0. \quad (24)$$

Orbits are classified based on the behaviour of $f(u)$ and $g(v)$. The most general form of $f(u)$ is attained for $\gamma C < 4a^2 E$. In such a circumstance, $f(u)$ has a local maximum at $u = 0$, $f_M = f(0) = C$, and a global minimum at $u = u_m$, $f_m = f(u_m)$, where

$$\cosh u_m = \left(\frac{4a^2 E}{C\gamma} \right)^{\frac{1}{\gamma-2}}, \quad (25)$$

and

$$f_m = -2a^2 E \sinh^2 u_m + C(\cosh u_m)^\gamma. \quad (26)$$

From (23) we obtain

$$I_2 \geq f_m. \quad (27)$$

On the other hand, $g(v)$ has a global maximum at $v = \pi$, $g_M = g(\pi) = \beta C$, and two global minima at $v = \pi/2$ and $v = 3\pi/2$, $g_m = g(\pi/2) = g(3\pi/2) = -2a^2 E$. Therefore, Inequality (24) implies

$$I_2 \leq 2a^2E. \quad (28)$$

By combining (27) and (28) one achieves

$$f_m \leq I_2 \leq 2a^2E. \quad (29)$$

By taking $2 < \gamma < 3$ and $\gamma C < 4a^2E$ into account, we arrive at $2a^2E > C$. Furthermore, f_m and in consequence I_2 , can take both positive and negative values. For a specified value of E , the following types of orbits occur as I_2 varies.

(i) *Butterflies*. For $C \leq I_2 < 2a^2E$, the allowed values for u and v are

$$u \leq u_0, \quad v_{b,1} \leq v \leq v_{b,2}, \quad v_{b,3} \leq v \leq v_{b,4}, \quad (30)$$

where u_0 and $v_{b,i}$ ($i = 1, 2, 3, 4$) are the roots of $f(u) = I_2$ and $g(v) = -I_2$, respectively. As Fig. 3a shows, the horizontal line that indicates the level of I_2 , intersects the graph of $f(u)$ at one point, which specifies the value of u_0 . The line corresponding to the level of $-I_2$ intersects $g(v)$ at four points that give the values of $v_{b,i}$ s (Fig. 3b). In this case the motion takes place in a region bounded by the coordinate curves $u = u_0$ and $v = v_{b,i}$. The orbits fill the shaded region of Fig. 4a. These are butterfly orbits (de Zeeuw 1985) that appear around the local minimum of Φ at $(x = 0, y = 0)$.

(ii) *Nucleophilic Bananas*. For $\beta C \leq I_2 < C$ the equation $f(u) = I_2$ has two roots, $u_{n,1}$ and $u_{n,2}$, which can be identified by the intersections of $f(u)$ and the level line of I_2 (see Fig. 3c). In this case, the equation $g(v) = -I_2$ has four real roots, $v = v_{n,i}$ ($i = 1, 2, 3, 4$), (Fig. 3d). The allowed ranges of u and v will be

$$u_{n,1} \leq u \leq u_{n,2}, \quad v_{n,1} \leq v \leq v_{n,2}, \quad v_{n,3} \leq v \leq v_{n,4}. \quad (31)$$

The orbits (Fig. 4b) are bound to the curves of $u = u_{n,1}$, $u = u_{n,2}$ and $v = v_{n,i}$. We call them nucleophilic banana orbits, for they look like banana and bend toward the nuclei.

(iii) *Horseshoes*. For $-\beta C \leq I_2 < \beta C$, both of the equations $f(u) = I_2$ and $g(v) = -I_2$ have two real roots. We denote these roots by $u = u_{h,i}$ and $v = v_{h,i}$ ($i = 1, 2$). In other words, the level lines of $\pm I_2$ intersect the graphs of $f(u)$ and $g(v)$ at two points as shown in Figs. 3e and 3f. The trajectories of stars fill the shaded region of Fig. 4c. We call these horseshoe orbits.

(iv) *Aligned Loops*. For $f_m < I_2 < -\beta C$, the equation $f(u) = I_2$ has two real roots, $u = u_{l,i}$ ($i = 1, 2$) while the equation $g(v) = -I_2$ has no real roots and Inequality (24) is always satisfied (Figs. 3g and 3h). The orbits fill a tubular region as shown in Fig. 4d. We call these aligned loops because they are aligned with the surface density isocontours of outer regions.

(v) *Transitional cases*. For $I_2 = 2a^2E$, stars undergo a rectilinear motion on the y -axis with the amplitude of $\pm a \sinh u_0$. For $I_2 = f_m$, loop orbits are squeezed to an elliptical orbit defined by $u = u_m$. For $\beta = 0$, horseshoe orbits are absent, leaving the other types of orbits symmetric with respect to the coordinate axes. Banana orbits no longer survive for $\beta = 1$ (eccentric disc model). In this case, butterflies extend to a *lens* orbit when $I_2 = C$ (see Figure 4e). For $\gamma C > 4a^2E$, $f(u)$ is a monotonically increasing function of u and ‘‘low-energy’’ butterflies are the only existing family of orbits. These are small-amplitude liberations in the vicinity of the local minimum of Φ at $(x = 0, y = 0)$.

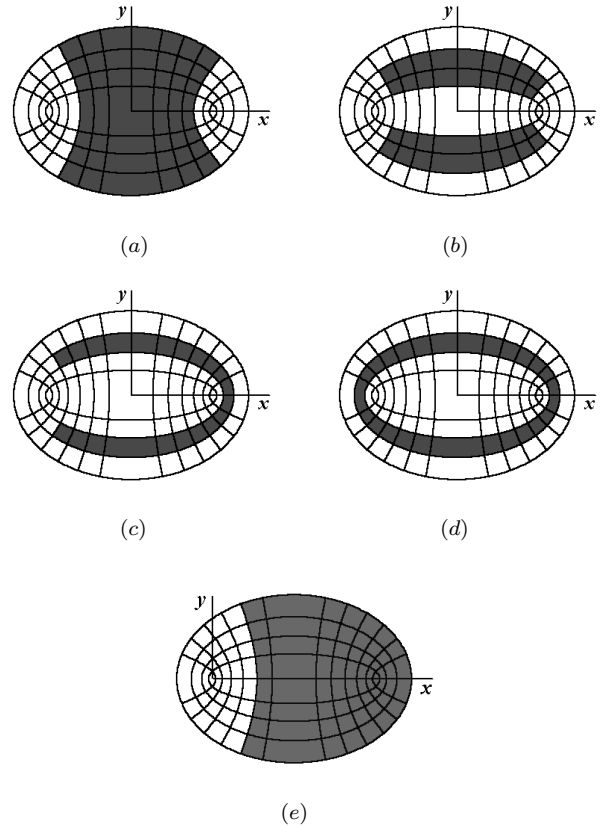


Figure 4. The possible families of orbits: (a) a butterfly orbit (b) nucleophilic banana orbits (c) a horseshoe orbit (d) an aligned loop orbit (e) a lens orbit associated with $\beta = 1$ and $I_2 = C$. For $\beta \neq 0$, the orbits are only symmetric with respect to the x -axis. Loop orbits are exceptional; they are always symmetric with respect to the coordinate axes.

4 THE POSITIVENESS OF THE SURFACE DENSITY

The sign of Σ is linked to that of $\nabla^2\Phi$ through Equation (3). To prove that Σ takes positive values for the potentials of (1), it suffices to show that the Laplacian of Φ is a positive function of γ , β , u and v .

Consider the Laplace equation in elliptic coordinates as

$$\nabla^2\Phi = \frac{1}{a^2D} (\Phi_{,uu} + \Phi_{,vv}), \quad (32)$$

$$D = \sinh^2 u + \sin^2 v,$$

where $,_s$ denotes $\frac{\partial}{\partial s}$. Substituting from (16) into (32), leads to

$$\nabla^2\Phi = \frac{\mathcal{F}(\gamma, \beta; u, v)}{2a^4D^4}, \quad (33)$$

with

$$\begin{aligned} \mathcal{F} = & D^2(F_{,uu} + G_{,vv}) - D(F + G)(D_{,uu} + D_{,vv}) \\ & - 2D(F_{,u}D_{,u} + G_{,v}D_{,v}) \\ & + 2(F + G)(D_{,u}^2 + D_{,v}^2). \end{aligned} \quad (34)$$

For the sake of simplicity, we assume $C = 1$. We show that the minimum of \mathcal{F} is always positive. We prove our claim for $-\frac{\pi}{2} \leq v \leq \frac{\pi}{2}$, which implies $G(v) = -\beta \cos^\gamma v$ (a similar method can be repeated for $\frac{\pi}{2} < v < \frac{3\pi}{2}$). In

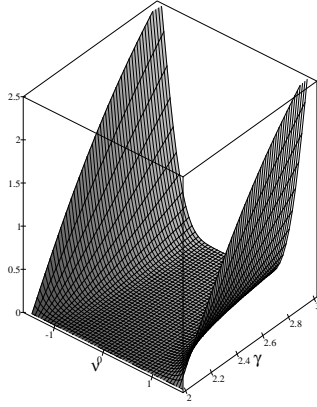


Figure 5. The behaviour of $\mathcal{G}(\gamma, v)$ for $-\frac{\pi}{2} \leq v \leq \frac{\pi}{2}$ and $2 < \gamma < 3$.

this case, \mathcal{F} will be a linear, decreasing function of β (because Φ has such a property). Therefore, one concludes $\mathcal{F}(\gamma, 1; u, v) \leq \mathcal{F}(\gamma, \beta; u, v)$. Furthermore, \mathcal{F} directly depends on $\cosh u$, which results in $\mathcal{F}(\gamma, 1; 0, v) \leq \mathcal{F}(\gamma, 1; u, v)$. Hence, $\nabla^2 \Phi$ is positive if $\mathcal{G}(\gamma, v) \equiv \mathcal{F}(\gamma, 1; 0, v) \geq 0$. By the evaluation of (34) for $\beta = 1$ and $u = 0$, one finds out

$$\begin{aligned} \mathcal{G}(\gamma, v) &= -\gamma^2 \sin^6 v \cos^{\gamma-1} v + \sin^2 v (1 - \cos^\gamma v) \\ &\quad + \gamma [\sin^4 v + \cos^{\gamma-2} v (\sin^6 v \\ &\quad - 3 \cos^2 v \sin^4 v)]. \end{aligned} \quad (35)$$

We have plotted $\mathcal{G}(\gamma, v)$ in Figure 5. On the evidence of this figure, \mathcal{G} is a positive function for $-\frac{\pi}{2} \leq v \leq \frac{\pi}{2}$ and $2 < \gamma < 3$. Thus, the surface density distribution takes positive values for all of our model galaxies.

5 DISCUSSION

In his pioneering work, Euler showed the separability of motion in the potential field of two *fixed* Newtonian centres of attraction. This problem was then completely solved by Jacobi (Pars 1965). It is physically impossible to keep apart these two ‘‘point masses’’, for they will attract each other leading to an eventual collapse. However, the assumed masses can be in equilibrium if they revolve around their common centre of mass (this is the classical 3-body problem). Our planar model is indeed Jacobi’s problem in which we have replaced two fixed centres of gravitation with a continuous distribution of matter, where mass concentration increases towards two nuclei (P1 and P2) in power-law, strong cusps. These nuclei are maintained by an interesting family of orbits, nucleophilic bananas. Below, we explain why the mentioned nuclei are generated and don’t collapse.

The force exerted on a star is equal to $-\nabla \Phi$. The motion under the influence of this force can be tracked on the *potential hill* of Figure 2a. This helps us to better imagine the motion trajectories.

5.1 The behaviour of orbits

Stars moving in nucleophilic banana orbits undergo motions *near* the 1:2 resonance. They oscillate twice in the y -direction for each x -axial oscillation. The turning points

of this group of stars lie on the curves $v = v_{n,i}$. These hyperbolic curves can be chosen arbitrarily close to P1 or P2. When stars approach P1 (or P2), their motion slows down (because they climb on the cuspy portion of the potential hill and considerably lose their kinetic energy while the potential energy takes a maximum) and the orbital angular momentum switches sign somewhere on $v = v_{n,i}$. Thus, these stars spend much time in the vicinity of P1 (or P2) and deposit a large amount of mass. This phenomenon is the main reason for the generation of cuspy zones around P1 and P2. Stars moving in nucleophilic bananas cross the y -axis quickly, and therefore, don’t contribute much mass to the region between the nuclei.

Horseshoe orbits cause the sizes of cuspy zones to be different through the following mechanism. Stars that start their motion sufficiently close to P1 (larger nucleus), are repelled from P1 because the force vector is not directed inward in this region. As they move outward, their orbits are bent and cross the x -axis with non-zero angular momentum. These stars linger only near P1, and in consequence, help the cuspy zone around P1 grow more than that of P2. The asymmetry of nucleophilic bananas, with respect to the y -axis, is also an origin of the different sizes of cuspy zones. In fact, horseshoe orbits are born once nucleophilic bananas join together for $I_2 = \beta C$. Horseshoe and nucleophilic banana orbits are the especial classes of boxlets that appropriately bend toward the nuclei. The lack of such a property in centrophobic banana orbits causes the discs of Sirdhar & Touma (1997) to be non-self-consistent.

Aligned loop orbits occur when the orbital angular momentum is high enough to prevent the test particle to slip down on the potential hill. The boundaries of loop orbits are defined by the ellipses $u = u_{l,1}$ and $u = u_{l,2}$. The nuclear cusps are located at the foci of these ellipses. Aligned loops have the same orientation as the surface density isocontours (compare Figures 1 and 4d). Thus, according to the results of Z99, it is possible to construct a self-consistent model using aligned loop orbits.

It is worthy to note that butterfly orbits play a significant role in maintaining the non-axisymmetric structure of the model at the moderate distances of $\mathcal{O}(a)$.

5.2 The nature of P1 and P2

The points where the cusps have been located, are inherently unstable. With a small disturbance, stars located at $(x = \pm a, y = 0)$ are repelled from these points because $-\nabla \Phi$ is directed outward when $r_i \rightarrow 0$ ($i = 1, 2$). But, the time that stars spend near the nuclei will be much longer than that of distant regions when they move in horseshoe and banana orbits. The points P1 and P2 are unreachable, for they correspond to the energy level $E = +\infty$. Based on the results of this paper, we conjecture that there may not be any mass concentration just at the centre of cuspy galaxies. However, a very dense region exists *arbitrarily* close to the centre!

5.3 The double nucleus can be in equilibrium

The nuclei pull each other due to their mutual gravitational attraction and it seems that they must collapse. However, we

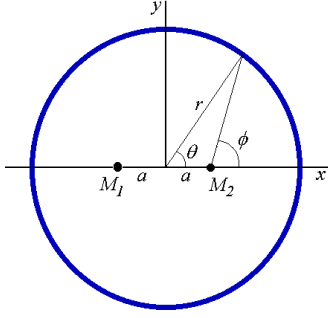


Figure 6. In this figure we have shown a circular ring of matter of outer regions. The masses of cuspy zones can approximately be computed and concentrated at the points $(\pm a, 0)$. The gravitational attraction of the ring upon the point mass M_1 (M_2) is directed in the x -direction due to the existing symmetry.

explain that in certain circumstances, the double nucleus can be in *static* equilibrium. At first we estimate the mass inside the separatrices of the surface density distribution (the mass of cuspy zones) and concentrate the matter at P1 and P2 (this is logical because the surface density distribution is almost axisymmetric near the nuclei). In this way, we obtain two point masses, M_1 and M_2 . According to (7) and (9), the following relations approximately hold

$$\begin{aligned} M_i &= \int_{-\pi}^{\pi} \int_{\epsilon}^{r_{0i}} \sigma_i r^{-1} dr d\theta, \quad \epsilon \rightarrow 0, \\ &= 2\pi\sigma_i \log \frac{r_{0i}}{\epsilon}, \quad i = 1, 2, \end{aligned} \quad (36)$$

where r_{0i} are chosen as the radii of inner tangent circles to the separatrices and the constant parameters σ_i are computed based on the surface density profile near the nuclei. As $\epsilon \rightarrow 0$, M_i s diverge to infinity unless a negative mechanism prevents them to grow. Consider the discs of radius ϵ with the centres located at $(\pm a, 0)$ and call them \mathcal{D}_1 and \mathcal{D}_2 . Since P1 and P2 are “locally” unstable, we rely on our previous argument that the matter is swept out from these points, allowing us to exclude \mathcal{D}_1 and \mathcal{D}_2 from our model for some $0 < \epsilon \ll 1$. In this way, M_i s take finite values.

M_1 and M_2 attract each other and start to move if they are not influenced by other gravitational sources. We claim that the required extra force comes from the gravitational attraction of the matter of outer regions. Consider Figure 6 where M_1 and M_2 are shown along with a ring of matter of outer regions. For brevity, we assume $\beta = 0$, which yields $M_1 = M_2 = M$. Due to the existing symmetry, the gravitational force exerted on M_2 by the assumed ring will have a resultant in the x -direction. When r is sufficiently large, $r \gg a$, this force is calculated as follows

$$F_x(r) = GM\sigma_{\infty} \int_{-\pi}^{\pi} \frac{r^{\gamma-2} \cos \phi d\theta}{r^2 + a^2 - 2ar \cos \theta}, \quad (37)$$

$$\cos \phi = \frac{r \cos \theta - a}{(r^2 + a^2 - 2ar \cos \theta)^{1/2}}, \quad (38)$$

where we have used $\Sigma \approx \sigma_{\infty} r^{\gamma-3}$ with σ_{∞} being a positive constant (see Eq. (11)). By integrating $F_x(r)$ over r from some $r = R \gg a$ to $r = \infty$, the total force, due to the matter of outer regions, is found to be

$$F_x = GM\sigma_{\infty} \int_R^{\infty} \int_{-\pi}^{\pi} \frac{r^{\gamma-2} (r \cos \theta - a) d\theta dr}{(r^2 + a^2 - 2ar \cos \theta)^{3/2}}. \quad (39)$$

By a change of independent variable as $\xi = a/r$, the integrand can be simplified in the form

$$F_x = b \int_0^{\xi_0} \xi^{2-\gamma} d\xi \frac{d}{d\xi} \int_0^{\pi} \frac{d\theta}{(1 + \xi^2 - 2\xi \cos \theta)^{1/2}}, \quad (40)$$

$$b = \frac{2GM\sigma_{\infty}}{a^{3-\gamma}}, \quad (41)$$

where $\xi_0 = a/R$. Consequently,

$$F_x = b \int_0^{\xi_0} \xi^{2-\gamma} d\xi \frac{d}{d\xi} \sum_{n=0}^{\infty} \xi^n \int_0^{\pi} P_n(\cos \theta) d\theta, \quad (42)$$

with P_n s being the well known Legendre functions. According to (Morse & Feshbach 1953)

$$\int_0^{\pi} P_{2k+1}(\cos \theta) d\theta = 0, \quad (43)$$

$$\int_0^{\pi} P_{2k}(\cos \theta) d\theta = \pi \left[\frac{(2k)!}{(2^k k!)^2} \right]^2 \equiv c_{2k}, \quad (44)$$

one achieves

$$F_x = b \int_0^{\xi_0} (\xi^{2-\gamma} \sum_{k=1}^{\infty} 2k c_{2k} \xi^{2k-1}) d\xi. \quad (45)$$

Integrating (45) over ξ , yields

$$F_x = bQ(\xi_0), \quad (46)$$

$$Q(\xi_0) = \xi_0^{2-\gamma} \sum_{k=1}^{\infty} \frac{2k c_{2k}}{2k + 2 - \gamma} \xi_0^{2k}. \quad (47)$$

It is obvious that Q is a positive function of ξ_0 . Therefore, from (46) one concludes $F_x > 0$ indicating that M_2 is pulled away from the centre. M_2 will be in static equilibrium if F_x is balanced with the gravitational force of M_1 , i.e.,

$$F_x = \frac{GM_1 M_2}{(2a)^2} = \frac{GM^2}{(2a)^2}. \quad (48)$$

By substituting from (36) and (46) into (48), we obtain

$$\delta \equiv \frac{\epsilon}{r_{01}} = e^{-s}, \quad s > 0, \quad (49)$$

where $r_{01} = r_{02}$, $\sigma_1 = \sigma_2$ (because we assumed $\beta = 0$) and

$$s = \frac{4\sigma_{\infty} a^{\gamma-1} Q(\xi_0)}{\pi \sigma_1}. \quad (50)$$

Our numerical computations of Σ reveal that $\sigma_{\infty} \gg \sigma_i$, which guarantees $\epsilon \ll r_{01}$ as desired. Following a similar procedure as above, one can show that the double nucleus remains in equilibrium for $\beta > 0$.

5.4 The nuclei of M31 and NGC4486B

In many respects, the surface density isocontours of our model galaxies are similar to the isophotal lines of the nuclei of M31 and NGC4486B. Our mass models are cuspy within two separatrices. Such curves can be distinguished in the nuclei of M31 and NGC4486B (see L96 and T95). We are not sure that the nuclei of M31 and NGC4486B are really cuspy, because existing telescopes can not highly resolve the regions around P1 and P2 (even HST images contain “few”

bright pixels at the locations of P1 and P2). Whatever the mass distribution inside these nuclei may be, our models reveal that double nuclei can exist even in the absence of supermassive BHs.

The nucleus of M31 can also be explained by the eccentric disc corresponding to $\beta = 1$. In such a circumstance, stars moving in butterfly orbits form a local group in the vicinity of $(x = 0, y = 0)$. The accumulation of stars around this local minimum of Φ can create a faint nucleus like P2 (see T95). Therefore, P2 will approximately be located at the “centre” of loop orbits while the eccentric, brighter nucleus (P1) is at the location of the cusp. In other words, loop and high-energy butterfly orbits will control the overall shape of outer regions, horseshoe orbits will generate P1 and low-energy butterflies will create P2.

5.5 Challenging problems

It is not known for us if there are rotationally supported double structures or not. This idea comes from the fact that we can replace the point masses of the restricted 3-body problem (the restricted 3-body problem is usually expressed in a rotating frame) with a continuous distribution of matter. Moreover, NGC4486B and the bulge of M31, are three dimensional objects and the assumption of planar models seems to be a severe constraint.

So far we showed that the double nucleus can be in static equilibrium due to the existing gravitational effects of the model. The stability study of such states, however, remains as a challenging problem.

Our next goal is to apply the method of Schwarzschild (1979,1993) for the investigation of self-consistency.

6 ACKNOWLEDGMENTS

The authors wish to thank the anonymous referee for illuminating questions and valuable comments on the paper.

REFERENCES

- Binney J., Tremaine S., 1987, *Galactic Dynamics*, Princeton University Press, Princeton
- de Zeeuw P.T., 1985, *MNRAS*, 216, 273
- Gerhard O.E., Binney J., 1985, *MNRAS*, 216, 467
- Goodman J., Binney J., 1984, *MNRAS*, 207, 511
- Jalali M.A., 1999, *MNRAS*, 310, 97 (J99)
- Lauer T.R., et al., 1996, *ApJ*, 471, L79 (L96)
- Merritt D., Quinlan G.D., 1998, *ApJ*, 498, 625
- Merritt D., Valluri M., 1996, *ApJ*, 471, 82
- Morse, P. M., Feshbach, H., 1953, *Methods of Theoretical Physics*, McGraw Hill, New York, Ch. 10
- Pars L.A., 1965, *A Treatise on Analytical Dynamics*, John Wiley & Sons, Inc., New York
- Schwarzschild M., 1979, *ApJ*, 232, 236
- Schwarzschild M., 1993, *ApJ*, 409, 563
- Sridhar S., Touma J., 1997, *MNRAS*, 287, L1-L4
- Tremaine S., 1995, *AJ*, 110, 628 (T95)
- Zhao H.S., Carollo C.M. & de Zeeuw P.T., 1999, *MNRAS*, 304, 457 (Z99)